RESEARCH ARTICLE | JUNE 21 2022

Spatially and spectrally resolved multicore optical fiber sensor with polarization sensitivity

Y. Hou ; Y. Jung

AIP Advances 12, 065023 (2022)
https://doi.org/10.1063/5.0095297

Spatially and spectrally resolved multicore optical fiber sensor with polarization sensitivity

Cite as: AIP Advances 12, 065023 (2022); doi: 10.1063/5.0095297
Submitted: 11 April 2022 • Accepted: 30 May 2022 •
Published Online: 21 June 2022

Y. Hou[a] and Y. Jung

AFFILIATIONS

Optoelectronics Research Centre, The University of Southampton, Southampton SO17 1BJ, United Kingdom

[a]Author to whom correspondence should be addressed: yaonan.hou@soton.ac.uk

ABSTRACT

We design and fabricate a multicore fiber sensor with the end facets of cores patterned with one-dimensional sub-wavelength Au wire grid polarizers, which are aligned either radially or azimuthally on the cross section of the fiber. With a fan-out device bridging the individual cores and external single core fibers followed by a compact spectrometer, it is able to spatially detect the light intensity, spectrum, and polarization states of the incident light in a highly integrated format. These multicore fiber sensors offer a new opportunity to simultaneously measure multiple optical parameters by a single operation.

Optical fiber sensors have drawn enormous attention owing to their vastly civil and military application with the advantages of high sensitivity, compactness, light weight and immunity to electromagnetic interference, accessibility to harsh environments, and so on.[1–3] Among various types of optical fiber sensors, micro-/nanostructures fabricated on the end facets of fiber cores demonstrate great potential toward the concept of "lab-on-fiber."[4] Compared with the widely studied single core fiber sensors with micro-patterned end facets, multicore fiber (MCF) sensors are emerging as a new platform with multiple waveguide channels and an additional spatial resolving capability,[5] while maintaining the fiber flexibility and compact device footprint. For this reason, MCF sensors are used in a wide range of imaging,[6] endoscopy,[7,8] and accurate detection of chemical or physical variants (e.g., vapors, displacement, temperature, and strain).[4,9–12] On the other hand, polarization analysis plays an important role in many practical applications (e.g., biochemical process), and it can provide additional information of the analytes. In particular, recent advances in structured lights with polarization vortices demand spatially resolved and polarization-sensitive sensing systems.[13,14] In addition, optical metasurfaces have attracted extensive interest to detect or manipulate the polarization state of the light and a few research groups have focused on advancing the polarization detection with planar sub-wavelength polarization filters.[15] To this end, the wire grid polarizer (WGP) is an appropriate candidate, which is composed of one-dimensional sub-wavelength gratings, favored by the fabrication process. A WGP allows the incident light with polarization perpendicular to the gratings to transmit, while the polarization parallel to the grating is reflected. Because of the availability of the structure by the state-of-the-art fabrications, WGPs are viable to be integrated with many optical devices, including light-emitting diodes,[16,17] lasers,[18] photo-detectors,[19] liquid crystal displays,[20] and cameras.[21–23] However, integration of WGPs with MCFs to realize spatially resolved optical measurements has not been reported.

In this work, we introduce a MCF sensor with each core integrated with an individual WGP, whose orientation is aligned along either radial or azimuthal directions. The cores are fanned-out with multiple single core fibers plugged into a compact spectrometer to measure the intensity and spectrum. Hence, the polarization of the incident beam can be spatially determined and analyzed. As a proof-of-concept experiment, an uncoupled 7-core fiber sensor was fabricated to analyze the optical properties of a vortex beam.

The photo in Fig. 1(a) displays the architecture of our MCF sensor, where the distal end fiber works as a detector head. The MCF has 7 cores, with 6 of them distributed on the vertices of a hexagon and 1 in the center [as shown in the left inset of Fig. 1(a)], with a core size of 8 μm, a core-to-core pitch of 50 μm, and a cladding diameter of 198 μm. The cores are numbered in sequence as shown in the inset of Fig. 1(a), where the central core is used

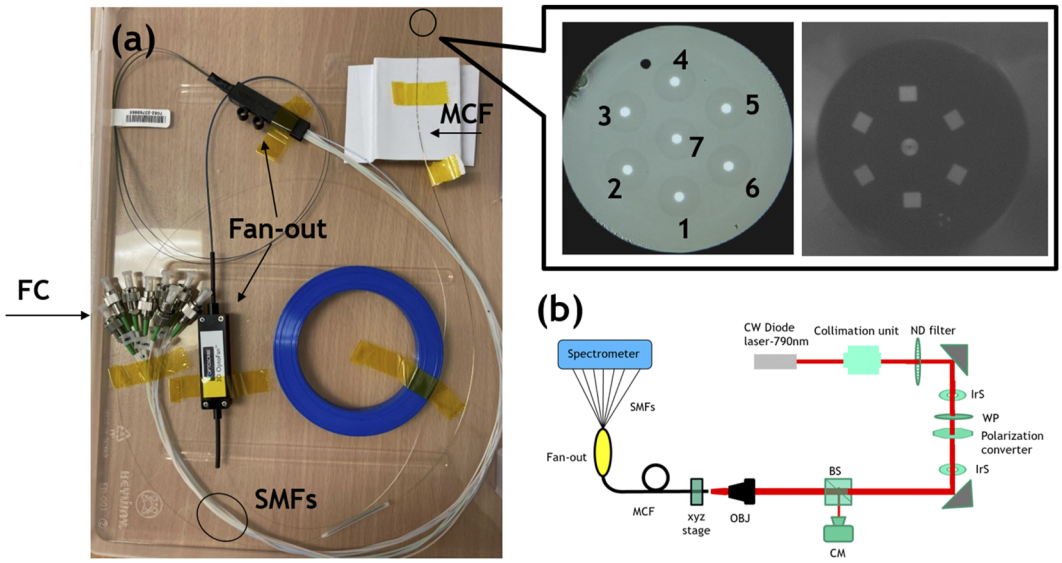

FIG. 1. (a) Structure of the MCF sensor, where the fan-out, SMF, and FC connectors are shown. The inset shows the facet of the MCF before (left) and after (right) coating with Au WGPs, where the numbers of the cores are labeled. The commercial single mode fibers (SMFs) act as single core fibers after fan-out. (b) Schematic of the system to characterize the MCF sensors.

for the alignment purpose and the remaining 6 cores are used for simultaneous optical detection. The right inset of Fig. 1(a) exemplifies Au WGPs inscribed into the Au film coated on the cores. The area of each WGP is 16 × 16 μm^2 so that the core is fully overlaid. The MCF is connected with a fan-out device followed by seven single core fibers. Figure 1(b) schematically shows the optical system used to characterize the MCF sensor. A continuous wave 785 nm diode laser (RLTMDL-785-100-5, Roithner Lasertechnik GmbH) is employed as an excitation source. The collimated beam is sent through a neutral density (ND) filter to adjust the intensity, and a subsequent $\lambda/2$-wave plate (WP) is used to manipulate the orientation of the linear polarization. An optional polarization converter (radial polarization converters, Edmund Optics, Inc.) can translate the incident light to spatially variant polarized beam (donut beam) and further propagates through a beam splitter. A 20× objective lens (OBJ) is used to focus the light to the end facet of the MCF, and the collected light from the single core fibers is recorded by a spectrometer (USB4000 Fiber Optic Spectrometer, Ocean optics). In order to fabricate an appropriate WGP, we first ran a simulation to find the best parameters by COMSOL multiphysics. In particular, we focus on the polarization extinction ratio (PER), defined as the transmission of p-polarized light [polarization perpendicular to the gratings, Fig. 2(c)] to that of s-polarized light and found that the anomalous diffusion starts to appear when the period is larger than 500 nm. On the other hand, the extinction ratio can be less than 20 dB at short wavelengths if the thickness is less than 250 nm, which is similar to previous reports.[19] Note that the extinction ratio can be reduced by any imperfections of nano-fabrications (especially at the visible wavelengths). In our experiment, the period of 450 nm is chosen, while the thickness and gap are 300 and 150 nm in order to compromise the extinction ratio and the absolute transmitted power.[19] In the device fabrication, a 300 nm Au layer is first deposited on a pre-cleaved end facet of the MCF and the WGPs are fabricated by focused ion beam (FIB) milling. A pair of MCF sensors were fabricated, where the orientation of WGPs on each core is aligned radially [Fig. 2(a), labeled as S1] or azimuthally [Fig. 2(b), labeled as S2]. Figure 2(c) shows the scanning electron microscope (SEM) image of the top-view of our WGP. A clean sub-wavelength grating structure is observed without any visible defects. Figure 2(d) shows the cross-sectional SEM image of the gratings, where an inclined sidewall formed, often observed when thick films are etched by FIB. The gap distance is 166 nm at the air side and 83 nm at the fiber side. Figure 2(e) shows the simulated transmittance of s- and p-polarized light by taking into account the actual structure of our fabricated device.[24] Wavelength dependent light transmittance was observed over a wavelength range of 600–1000 nm but the calculated PER is more than 20 dB in the visible light region and >40 dB in the near infrared region. Note that it is important to have such a large PER in simulation because it will be inevitably reduced by manufacturing imperfections.[25] The measured transmittance of the WGPs fabricated on S1 and S2 is shown in Fig. 2(f) for both orthogonal polarizations. A small difference in transmittance of the two different gratings suggests good reproducibility in our manufacturing process. For both samples, the measured PERs were >13 dB across the entire wavelength range of 600–1000 nm. We believe that slightly reduced PER results from the limited dimensions of the actual device, compared to the infinite grating area used in the simulation, along with fabrication imperfections. Figure 2(g) shows the optical images of the WGPs under white light illumination from the back side, while a polarization analyzer is applied before the camera. It is observed that the pairs of gratings are lighted up in a complementary behavior with the analyzer aligned to 0°, 60°, and 120°, respectively. Figure 2(h) shows the normalized transmittance of both polarizers as a function of the angle of the analyzer. As expected,

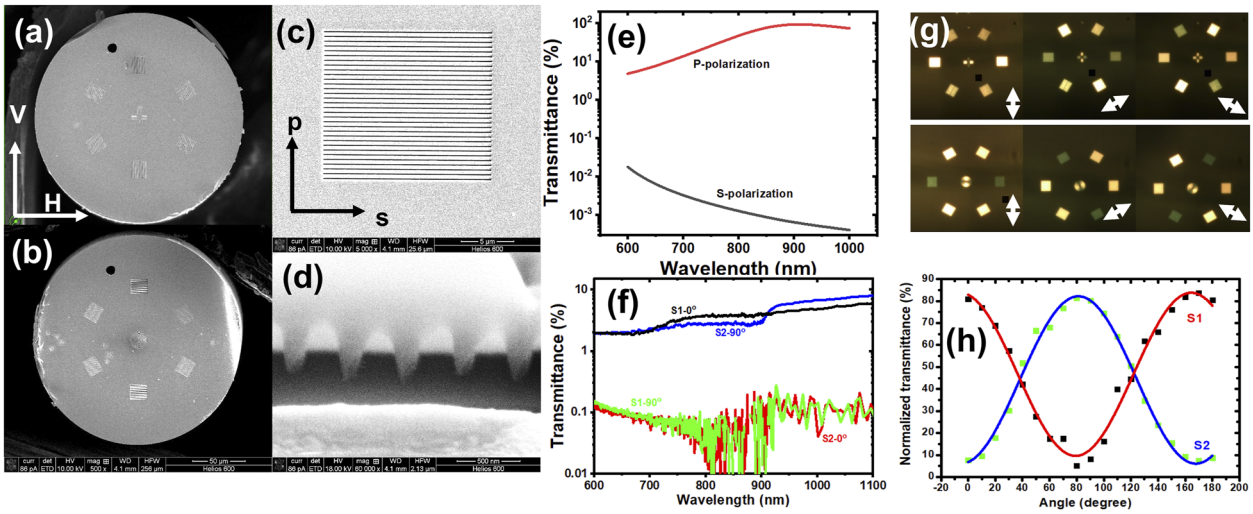

FIG. 2. SEM image of the WGPs fabricated on the end facet of the MCF aligned in (a) radial and (b) azimuthal directions (scale bar = 50 μm). SEM images of the top-view (c) and cross-sectional view (d) of the WBP (scale bar = 5 μm and 500 nm, respectively); simulated (e) and measured (f) transmittance of the gratings for two orthogonal states of linear polarized light on both S1 and S2 samples. (g) Optical images of the gratings with a polarization analyzer aligned in 0°, 60°, and 120°. (h) Transmittance of the WGP from S1 and S2 as a function of the analyzer angle [polarization angles in (f)–(h) are referred to those shown in (g)].

the experimental data of two orthogonal polarizers can be well fitted into a sinusoidal function with a period of π, but with an anti-phase behavior.

Note that the spatially distributed WGPs shown in Fig. 2(g) can be projected to a CCD camera and it is possible to determine the polarization from a single measurement with our devices. In order to do this, the optical properties of the MCF sensors are first characterized under linearly polarized light using the setup shown in Fig. 1(b). Figures 3(a) and 3(b) show the spectra collected by the cores of the two MCF sensors at the same relative position to the beam. Apart from the distinguished extinction ratio, the measured spectrum resembles one another. By measuring the optical power of

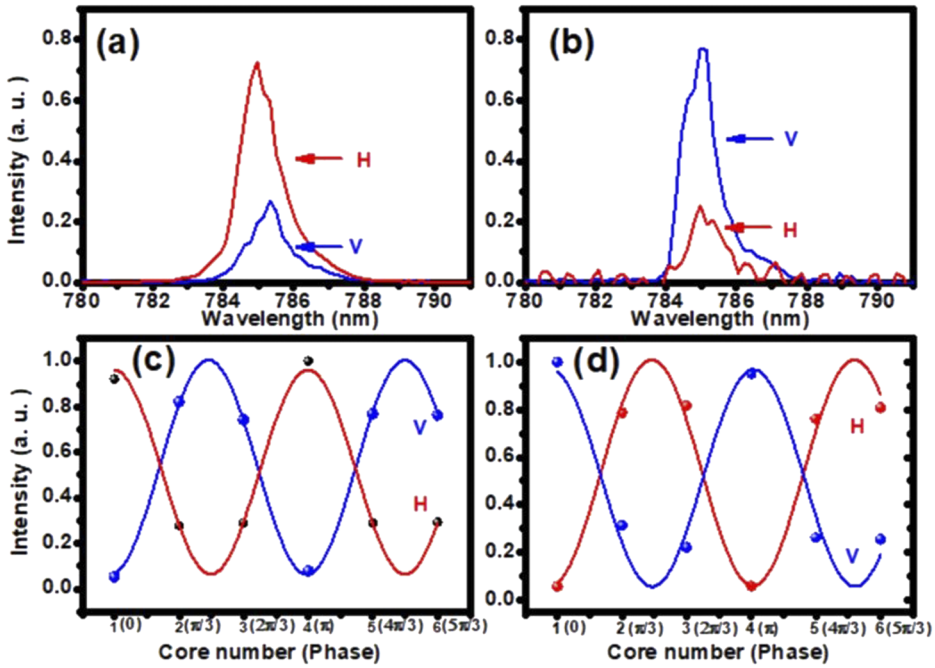

FIG. 3. The spectra of the incident light from core 6 in S1 (a) and S2 (b). Normalized intensity as a function of the spatially distributed cores of S1 (c) and S2 (d) under linear polarizations. [H: horizontal polarization; V: vertical polarization. The polarization directions are defined in Fig. 2(a).]

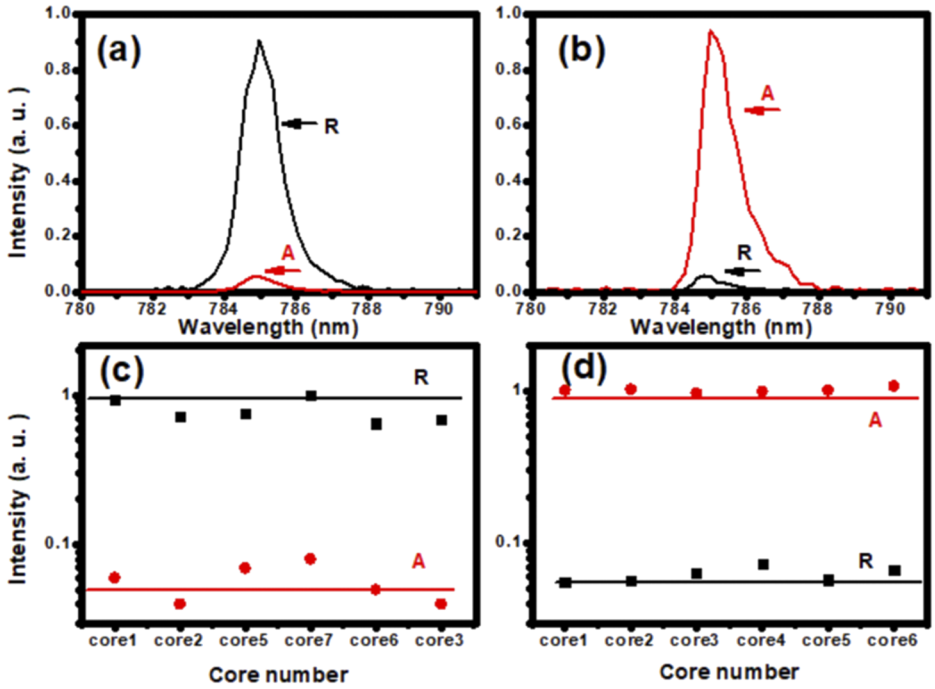

FIG. 4. The spectra of the incident light from core 6 in S1 (a) and S2 (b) under radial and azimuthal polarizations. Normalized intensity as a function of the spatially distributed cores of S1 (c) and S2 (d) under radial and azimuthal polarizations (R: radial polarization; A: azimuthal polarization).

the cores, spatially resolved spectroscopy can be obtained with our MCF sensor from a single capture. Figures 3(c) and 3(d) show normalized intensity through each core, which is numbered in sequence. The spatial distribution is translated into relative rotation angles with respect to core 1. For the same MCF sensor, the two curves are anti-phase as a result of the orthogonal polarization of the incident light. Under the same polarized light waves, the two devices also show an anti-phase behavior because of the orthogonal distribution of the WGPs. Similar to rotating a linear polarizer, each of the MCF sensors can be used to determine the orientation of linear polarization from a single measurement.

In the final part, we demonstrate the measurement of the spatial distribution of linear polarization with our device. In order to do this, a polarization converter was employed to generate polarization vertices, which is a key feature of many important optical beams/pulses including vector beams[26,27] and optical "flying donuts."[28,29] Figures 4(a) and 4(b) show the spectra obtained from two orthogonal cores on S1 and S2, respectively. The spectrum of S1 under azimuthal (radial) polarization is identical to that of S2 under radial (azimuthal) polarization, implying the function of polarized spectroscopy. Figures 4(c) and 4(d) show the normalized intensity of the azimuthal and radial polarized beams, measured with the 6 cores of S1 and S2. A good extinction ratio of 17 dB (18 dB) for S1 (S2) is obtained, agreeing well the value measured with a single WGP shown in Fig. 2(f). The results indicate that our devices are able to measure spatial distributed polarization.

In summary, we demonstrated a compact MCF sensor, having broadband WGPs patterned on the end facet of individual cores and aligned in azimuthal or radial orientations. Along with a plug-in spectrometer, our sensor can realize spatially resolved spectroscopy and polarization analysis from a single measurement. Despite the requirement of further improvement in the fabrication method to enhance the extinction ratio, our prototype MCF sensor with spatially resolved polarization sensitivity would be important for information technology, chemical analysis, and biological diagnostics. Also note that WGPs can be replaced by similar nanostructures, e.g., resonant gratings[30,31] or metasurfaces,[32] where it is likely to archive spectral filtering or full Stokes measurements.

This work was supported by the Research Stimulus Fund at the Zepler Institute for Photonics and Nanoelectronics, the University of Southampton, and partly by the Engineering and Physical Science Research Council under Grant Nos. EP/N00762X/1 and EP/T028475/1. The authors specially thank Dr. John Hayes for providing multicore fiber and Dr. Nikitas Papasimakis, Professor Dave Richardson, and Professor Nikolay I. Zheludev for the helpful discussions. For the purpose of open access, the authors have applied a creative commons attribution (CC BY) license [where permitted by UKRI, "open government licence" or "creative commons attribution no-derivatives (CC BY-ND) licence" may be stated instead] to any author accepted manuscript version arising.

AUTHOR DECLARATIONS

Conflict of Interest

The authors have no conflicts to disclose.

DATA AVAILABILITY

The data that support the findings of this study are available from the corresponding author upon reasonable request.

REFERENCES

[1] B. Lee, "Review of the present status of optical fiber sensors," Opt. Fiber Technol. **9**, 57–79 (2003).

[2] A. D. Kersey, "A review of recent developments in fiber optic sensor technology," Opt. Fiber Technol. **2**, 291–317 (1996).

[3] M. Yasin, S. W. Harun, and H. Arof, *Recent Progress in Optical Fiber Research* (IntechOpen, 2012).

[4] S. Zhang, S. J. Tang, S. Feng, Y. F. Xiao, W. Cui, X. Wang, W. Sun, J. Ye, P. Han, X. Zhang *et al.*, "High-q polymer microcavities integrated on a multicore fiber facet for vapor sensing," Adv. Opt. Mater. **7**, 1900602 (2019).

[5] V. Kamaljith, M. G. Tanner, H. A. C. Wood, K. Harrington, D. Choudhury, M. Bradley, and R. R. Thomson, "Ultrafast-laser-ablation-assisted spatially selective attachment of fluorescent sensors onto optical fibers," Opt. Lett. **45**, 2716–2719 (2020).

[6] S. Sivankutty, E. R. Andresen, G. Bouwmans, T. G. Brown, M. A. Alonso, and H. Rigneault, "Single-shot polarimetry imaging of multicore fiber," Opt. Lett. **41**, 2105–2108 (2016).

[7] J. Shin, D. N. Tran, J. R. Stroud, S. Chin, T. D. Tran, and M. A. Foster, "A minimally invasive lens-free computational microendoscope," Sci. Adv. **5**, eaaw5595 (2019).

[8] V. Tsvirkun, S. Sivankutty, G. Bouwmans, O. Katz, E. R. Andresen, and H. Rigneault, "Widefield lensless endoscopy with a multicore fiber," Opt. Lett. **41**, 4771–4774 (2016).

[9] Q. Liu, Y. Zhan, S. Zhang, S. Feng, X. Wang, W. Sun, J. Ye, and Y. Zhang, ""Optical tentacle" of suspended polymer micro-rings on a multicore fiber facet for vapor sensing," Opt. Express **28**, 11730–11741 (2020).

[10] C. Zhang, Z. Jiang, S. Fu, M. Tang, W. Tong, and D. Liu, "Femtosecond laser enabled selective micro-holes drilling on the multicore-fiber facet for displacement sensor application," Opt. Express **27**, 10777–10786 (2019).

[11] C. Zhang, S. Fu, M. Tang, and D. Liu, "Parallel Fabry-Perot interferometers fabricated on multicore-fiber for temperature and strain discriminative sensing," Opt. Express **28**, 3190–3199 (2020).

[12] H. Zhang, Z. Wu, P. P. Shum, X. Q. Dinh, C. W. Low, Z. Xu, R. Wang, X. Shao, S. Fu, W. Tong *et al.*, "Highly sensitive strain sensor based on helical structure combined with Mach-Zehnder interferometer in multicore fiber," Sci. Rep. **7**, 46633 (2017).

[13] M. McLaren, T. Konrad, and A. Forbes, "Measuring the nonseparability of vector vortex beams," Phys. Rev. A **92**, 023833 (2015).

[14] Y. Shen, X. Yang, D. Naidoo, X. Fu, and A. Forbes, "Structured ray-wave vector vortex beams in multiple degrees of freedom from a laser," Optica **7**, 820–831 (2020).

[15] Y. Intaravanne and X. Chen, "Recent advances in optical metasurfaces for polarization detection and engineered polarization profiles," Nanophotonics **9**, 1003 (2020).

[16] M. Ma, D. S. Meyaard, Q. Shan, J. Cho, E. F. Schubert, G. B. Kim, M.-H. Kim, and C. Sone, "Polarized light emission from GaInN light-emitting diodes embedded with subwavelength aluminum wire-grid polarizers," Appl. Phys. Lett. **101**, 061103 (2012).

[17] M. Wang, B. Cao, C. Wang, F. Xu, Y. Lou, J. Wang, and K. Xu, "High linearly polarized light emission from InGaN light-emitting diode with multilayer dielectric/metal wire-grid structure," Appl. Phys. Lett. **105**, 151113 (2014).

[18] H. Tamada, T. Doumuki, T. Yamaguchi, and S. Matsumoto, "Al wire-grid polarizer using the *s*-polarization resonance effect at the 0.8-μm-wavelength band," Opt. Lett. **22**, 419–421 (1997).

[19] M. Guillaumée, L. A. Dunbar, Ch. Santschi, E. Grenet, R. Eckert, O. J. F. Martin, and R. P. Stanley, "Polarization sensitive silicon photodiodes using nanostructured metallic grids," Appl. Phys. Lett. **94**, 193503 (2009).

[20] S. H. Kim, J.-D. Park, and K.-D. Lee, "Fabrication of a nano-wire grid polarizer for brightness enhancement in liquid crystal display," Nanotechnology **17**, 4436 (2006).

[21] V. Gruev, R. Perkins, and T. York, "CCD polarization imaging sensor with aluminum nanowire optical filters," Opt. Express **18**, 19087–19094 (2010).

[22] S. Im, G. Moon, and D. Kim, "Dispersive effects in imaging polarimetry based on a wire-grid polarizer," Sci. Rep. **10**, 9495 (2020).

[23] Y. Zhou and D. J. Klotzkin, "Design and parallel fabrication of wire-grid polarization arrays for polarization-resolved imaging at 1.55 μm," Appl. Opt. **47**, 3555–3560 (2008).

[24] G. Mélen, W. Rosenfeld, and H. Weinfurter, "Impact of the slit geometry on the performance of wire-grid polarisers," Opt. Express **23**, 32171–32178 (2015).

[25] T. Siefke, S. Kroker, K. Pfeiffer, O. Puffky, K. Dietrich, D. Franta, I. Ohlídal, A. Szeghalmi, E. B. Kley, and A. Tünnermann, "Materials pushing the application limits of wire grid polarizers further into the deep ultraviolet spectral range," Adv. Opt. Mater. **4**, 1780–1786 (2016).

[26] F. Gori, "Polarization basis for vortex beams," J. Opt. Soc. Am. A **18**, 1612–1617 (2001).

[27] B. Wang, W. Liu, M. Zhao, J. Wang, Y. Zhang, A. Chen, F. Guan, X. Liu, L. Shi, and J. Zi, "Generating optical vortex beams by momentum-space polarization vortices centred at bound states in the continuum," Nat. Photonics **14**, 623–628 (2020).

[28] T. Raybould, V. A. Fedotov, N. Papasimakis, I. Youngs, and N. I. Zheludev, "Exciting dynamic anapoles with electromagnetic doughnut pulses," Appl. Phys. Lett. **111**, 081104 (2017).

[29] N. Papasimakis, T. Raybould, V. A. Fedotov, D. P. Tsai, I. Youngs, and N. I. Zheludev, "Pulse generation scheme for flying electromagnetic doughnuts," Phys. Rev. B **97**, 201409 (2018).

[30] V. Savinov and N. I. Zheludev, "High-quality metamaterial dispersive grating on the facet of an optical fiber," Appl. Phys. Lett. **111**, 091106 (2017).

[31] C. Pelzman and S.-Y. Cho, "Multispectral and polarimetric photodetection using a plasmonic metasurface," J. Appl. Phys. **123**, 043107 (2018).

[32] N. A. Rubin, G. D'Aversa, P. Chevalier, Z. Shi, W. T. Chen, and F. Capasso, "Matrix Fourier optics enables a compact full-Stokes polarization camera," Science **365**, eaax1839 (2019).